

Theory of resonant inelastic x-ray scattering at the K edge in La_2CuO_4 - Multiple scattering effects -

Jun-ichi Igarashi¹, Takuji Nomura², and Manabu Takahashi³

¹*Faculty of Science, Ibaraki University, Mito, Ibaraki 310-8512, Japan*

²*Synchrotron Radiation Research Center,*

Japan Atomic Energy Research Agency, Hyogo 679-5148, Japan

³*Faculty of Engineering, Gunma University, Kiryu, Gunma 376-8515, Japan*

(Dated: December 2, 2024)

Abstract

We develop a theory of resonant inelastic x-ray scattering (RIXS) at the K edge in La_2CuO_4 on the basis of the Keldysh Green's function formalism. In our previous analysis (Phys. Rev. B 71, 035110(2005)), the scattering by the core-hole potential was treated within the Born approximation, and a crude model density of states was used for the $4p$ band. We improve the analysis by taking account of the multiple scattering in $\text{Cu}3d\text{-O}2p$ bands and by using a realistic $4p$ density of states (DOS) obtained from a band calculation. The multiple scattering effect is evaluated with the use of the time representation developed by Noziere and de Dominicis. It is found that the K -edge peak in the absorption coefficient moves to a lower energy region as a function of photon energy, and that the multiple-scattering effect on the RIXS spectra does not change the two-peak structure but modifies slightly the shape as a function of energy loss. These findings suggest that the multiple scattering effect could mainly be included into a renormalization of the core-level energy, and partly justify the Born approximation, leading to a future application to the RIXS in three-dimensional systems.

PACS numbers: 78.70.Ck, 74.72.Dn, 78.20.Bh

I. INTRODUCTION

Resonant inelastic x-ray scattering (RIXS), taking advantage of high intensity of synchrotron sources, has become a powerful tool to probe charge excitations in solids.^{1,2,3,4,5,6,7} The momentum dependence is detectable in transition-metal compounds by using the K edge resonance, because the wavelength of photon is an order of crystal lattice spacing. The spectra consist of several peaks as a function of energy loss, and the peak positions sometimes move with changing momenta transferred to the crystal. This is quite different from the optical conductivity,⁸ where the momentum transfer is limited to nearly zero. Electron energy loss spectroscopy can also detect the momentum dependence on charge excitations, but it suffers from strong multiple scattering effects.⁹ Therefore, RIXS is quite valuable to investigate charge excitations, which is comparable to the neutron inelastic scattering for detecting spin excitations.

In the RIXS process, the $1s$ core electron is prompted to an empty $4p$ state by absorbing photon, then charge excitations are created in order to screen the core-hole potential. Finally the photo-excited $4p$ electron is recombined with the core hole by emitting photon. Charge excitations are left with energy and momentum transferred from photon at the end. Most theoretical studies on the momentum dependence of the RIXS spectra in cuprates have been based on the numerical diagonalization method for small clusters. The $4p$ band was replaced by a single level there.^{10,11,12} A single band Hubbard model has been sometimes used with replacing the charge transfer band (so called “Zhang-Rice” band) by the lower Hubbard band in two-dimensional cases.^{10,12} It is not clear whether this replacement is appropriate, since the low energy peak is assigned to an excitation from the charge transfer band to the upper Hubbard band. The single band Hubbard model cannot describe another high energy peak, either.

By contrast, in our previous papers,^{13,14} we have formulated the RIXS spectra on the multi-band tight-binding model by adapting the resonant Raman theory developed by Noziere and Abrahams.¹⁵ The formalism was based on the Hartree-Fock approximation (HFA) to describe the electronic states in the antiferromagnetic (AF) phase and the random phase approximation (RPA) to the propagation of electron-hole pairs. The HFA is known to provide a good starting point for undoped materials. The calculation reinforced by the RPA correction has reproduced well the experimental RIXS spectra as a function of energy

loss and the dependence on momentum in La_2CuO_4 .¹⁴ Thus, the formula seems promising to analyze the RIXS spectra in more complicated systems in three dimensions. But it should be noted that we have used a crude model for the $4p$ band and have treated the core-hole potential in the intermediate state by the Born approximation with neglecting the multiple scattering effect. Since the core-hole potential is not weak, higher-order effects might be important. Therefore, it is desirable to check and improve the approximations made before going to further applications. One purpose of this paper is to address this issue by using a realistic $4p$ density of states obtained from the band calculation and by evaluating the higher-order effects. Another purpose of this paper is to give a detailed derivation of the formula of RIXS spectra, because details have been sketchy in our previous papers.^{13,14} We present the formula with an emphasis of the time representation.

We invent a numerical method to treat the multiple scattering by the core-hole potential along the line of Noziere and de Dominicis,¹⁶ deriving the Dyson equation to the one-electron Green's function with the core-hole potential working in finite time interval. The point is that, different from metallic systems, we can numerically solve the Dyson equation for insulating systems, because the equation has no singular term. On the basis of the solution, we evaluate the multiple scattering effects on the RIXS spectra as well as the absorption coefficient. This type of analysis has not been attempted before. In the absorption coefficient, it is found that the K -edge peak moves to the lower energy region due to screening, and that the intensity at a higher energy region is a little enhanced as anti-screening effect. When the incident photon energy is tuned at the K -edge peak, the RIXS spectra have peaks at around 2 eV and 5 eV as a function of energy loss. The 2eV-peak corresponds to the excitation of electron from the charge transfer band to the upper Hubbard band. It is found that the two-peak structure does not alter but the shape is slightly modified by the multiple scattering effect; the 2eV-peak is enhanced while the 5eV-peak is suppressed. The enhancement of the 2eV-peak is reasonable, because the core-hole potential is most likely to be screened by the excitation of electron from the charge transfer band to the upper Hubbard band in the intermediate state when the incident photon energy is tuned at the K edge. However, the multiple scattering effect is limited within a small correction in the RIXS spectra. This may partly justify the Born approximation after a renormalization of the core-level energy.

The present paper is organized as follows. In Sec. II, we introduce a model and formulate the RIXS spectra. In Sec. III, the electronic structure is calculated on the d - p model within

the HFA in the AF phase of La_2CuO_4 . The RIXS spectra are calculated within the Born approximation in comparison with the experiment in Sec. IV. The multiple scattering effect is evaluated on the absorption and the RIXS spectra in Sec. V. Section VI is devoted to the concluding remarks.

II. FORMULATION FOR RIXS SPECTRA

A. Description of model

We start by the expression of the Hamiltonian of photon,

$$H_{ph} = \sum_{\mathbf{q}\alpha} \omega_{\mathbf{q}} c_{\mathbf{q}\alpha}^\dagger c_{\mathbf{q}\alpha}, \quad (2.1)$$

where operator $c_{\mathbf{q}\alpha}$ represents the annihilation operator of photon with momentum \mathbf{q} , polarization α . For the interaction between photon and matter, we consider the dipole transition at the K edge, where the $1s$ -core electron is excited to the $4p$ band with absorbing photon and the reverse process takes place. This process may be described by

$$H_x = w \sum_{\mathbf{q}\alpha} \frac{1}{\sqrt{2\omega_{\mathbf{q}}}} \sum_{j\eta\sigma} e_{\eta}^{(\alpha)} p_{j\eta\sigma}'^\dagger s_{j\sigma} c_{\mathbf{q}\alpha} e^{i\mathbf{q}\cdot\mathbf{r}_j} + \text{H.c.}, \quad (2.2)$$

where $e_{\mu}^{(\alpha)}$ represents the η -th component ($\eta = x, y, z$) of two kinds of polarization vectors ($\alpha = 1, 2$) of photon. Since the $1s$ state is so localized that the $1s \rightarrow 4p$ dipole transition matrix element is well approximated as a constant w . Annihilation operators $p_{j\eta\sigma}'$ and $s_{j\sigma}$ are for states $4p_{\eta}$ and state $1s$ at Cu site j , respectively.

The Hamiltonians for the core electron and the $4p$ electron are given by

$$H_{1s} = \epsilon_{1s} \sum_{j\sigma} s_{j\sigma}^\dagger s_{j\sigma}, \quad (2.3)$$

$$H_{4p} = \sum_{\mathbf{k}\eta\sigma} \epsilon_{4p}^{\eta}(\mathbf{k}) p_{\mathbf{k}\eta\sigma}'^\dagger p_{\mathbf{k}\eta\sigma}'. \quad (2.4)$$

The photo-created $1s$ -core hole induces charge excitations through the attractive core-hole potential, which may be described by

$$H_{1s-3d} = V \sum_{j\sigma\sigma'} d_{j\sigma}^\dagger d_{j\sigma'} s_{j\sigma'}^\dagger s_{j\sigma}. \quad (2.5)$$

Here V may be 5–10 eV in La_2CuO_4 . We neglect the interaction between the core-hole and the 4p electron, since the 4p states are well extended in space with the band width as large as ~ 20 eV. The excited 4p electron is finally recombined with the core-hole with emitting photon. In the end, charge excitations remain with receiving a momentum and an energy from scattering photons.

In La_2CuO_4 , Cu and O atoms form a two-dimensional network shown in Fig. 1. There is nominally one hole per Cu atom. To describe this situation, we consider only the $x^2 - y^2$ orbital at Cu site, which hybridizes the σ -bonding 2p orbitals at O sites (“ d - p ” model). The corresponding Hamiltonian may be expressed as

$$\begin{aligned}
H_{dp} = & \epsilon_d \sum_{j\sigma} d_{j\sigma}^\dagger d_{j\sigma} + \epsilon_p \sum_{\ell\sigma} p_{\ell\sigma}^\dagger p_{\ell\sigma} \\
& + \sum_{j\ell\sigma} t_{j\ell} d_{j\sigma}^\dagger p_{\ell\sigma} + \text{H.c.} + \sum_{\ell\ell'\sigma} t_{\ell\ell'} p_{\ell\sigma}^\dagger p_{\ell'\sigma} \\
& + U_d \sum_j d_{j\uparrow}^\dagger d_{j\uparrow} d_{j\downarrow}^\dagger d_{j\downarrow},
\end{aligned} \tag{2.6}$$

where $d_{j\sigma}$ is the annihilation operator for the $x^2 - y^2$ orbital with spin σ at Cu site j , and $p_{\ell\sigma}$ is the annihilation operator of the 2p orbital with spin σ at site ℓ . For La_2CuO_4 , the transfer energies between 3d and 2p orbitals t_d and that between 2p orbitals t_p are estimated from the local density approximation (LDA) calculations, that is, $t_d = 1.3$ eV, $t_p = 0.65$ eV.¹⁷ We assume $U_d = 11$ eV, and the 3d level energy relative to the 2p level $\epsilon_d + \frac{1}{2}U_d n_d - \epsilon_p = -0.7$ eV with $n_d = \sum_\sigma \langle d_{j\sigma}^\dagger d_{j\sigma} \rangle$. These values are set the same as those in our previous paper.¹⁴

B. Keldysh-Schwinger formalism

Following Noziere and Abraham,¹⁵ we use the Keldysh-Schwinger formalism to the RIXS spectra. We prepare the initial state that one photon exists with \mathbf{q}_i , α_i in addition to a material in the ground state, which may be expressed as

$$|\Phi_i\rangle = c_{\mathbf{q}_i\alpha_i}^\dagger |0\rangle, \tag{2.7}$$

where $|0\rangle$ is the ground state of the matter with no photon. Let $H \equiv H_{ph} + H_{dp} + H_{1s} + H_{4p}$ be the unperturbed Hamiltonian of the system and H_x be the perturbation. Then the S -matrix is given by

$$U(t, -\infty) = T \exp \left\{ -i \int_{-\infty}^t H_x(t') dt' \right\}, \tag{2.8}$$

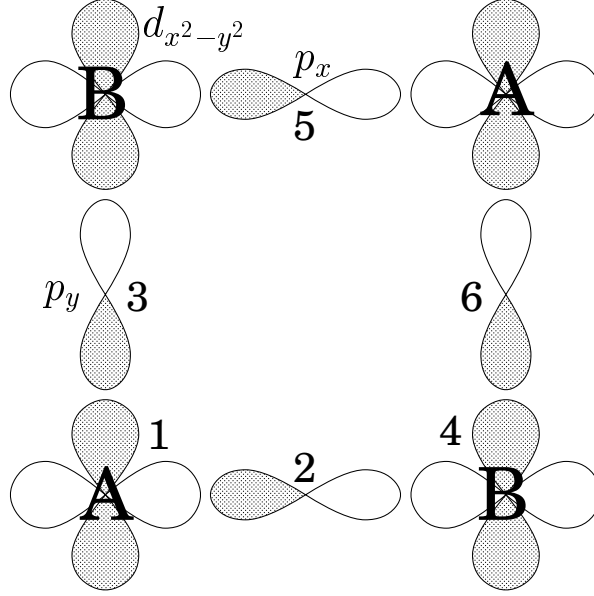


FIG. 1: Schematic view of the unit cell in the antiferromagnetic phase. Six orbitals (numbered 1-6) are considered. There are two nonequivalent sites of Cu shown as A and B. Gray parts in orbitals indicate that their wave functions take negative values.

with $H_x(t) = \exp(iHt)H_x\exp(-iHt)$. The probability of finding a photon with momentum \mathbf{q}_f , polarization α_f at time t_0 is given by

$$P_{\mathbf{q}_f\alpha_f;\mathbf{q}_i\alpha_i}(t_0) = \langle \Phi_i | U(-\infty, t_0) c_{\mathbf{q}_f\alpha_f}^\dagger c_{\mathbf{q}_f\alpha_f} U(t_0, -\infty) | \Phi_i \rangle. \quad (2.9)$$

Expanding the S-matrix to second order in H_x ,

$$\begin{aligned} U(t, -\infty) &= 1 + (-i) \int_{-\infty}^t H_x(t') dt' \\ &+ \frac{(-i)^2}{2} \int_{-\infty}^t \int_{-\infty}^t T(H_x(t') H_x(t'')) dt' dt'', \end{aligned} \quad (2.10)$$

we insert this into Eq. (2.9). Figure 2 shows a schematic representation of the expansion, where the wavy lines indicate photons which carry energy and momentum, and the solid lines with "4p" and "1s" represent the Green's functions of the 4p electron and the 1s core-hole, respectively. The upper and lower halves of the graph correspond to the so called "outward" and "backward" time legs, respectively. By factoring out the dependence on the photon frequencies, we obtain

$$P_{\mathbf{q}_f\alpha_f;\mathbf{q}_i\alpha_i}(t_0) = \int_{-\infty}^{t_0} du \int_{-\infty}^u dt \int_{-\infty}^{t_0} du' \int_{-\infty}^{u'} dt' S(t, u; t' u') e^{i\omega_i(t'-t)} e^{-i\omega_f(u'-u)}. \quad (2.11)$$

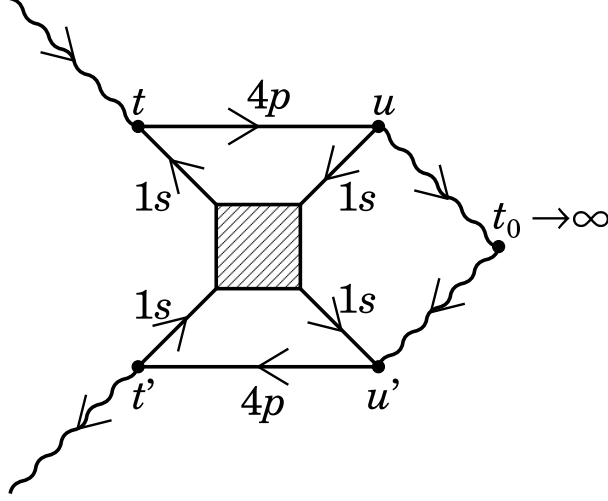


FIG. 2: Expansion of the S matrix. Wavy lines represent photon Green's functions. The solid lines with “4p” and “1s” represent Green's functions of the 4p electron and the 1s core-hole, respectively.

The transition probability per unit time with $t_0 \rightarrow \infty$ is given by fixing one time, for instance, $u = 0$:

$$W(q_f \alpha_f; q_i \alpha_i) = \int_{-\infty}^0 dt \int_{-\infty}^{\infty} du' \int_{-\infty}^{u'} dt' S(t, 0; t' u') e^{i\omega_i(t'-t)} e^{-i\omega_f u'}. \quad (2.12)$$

III. HARTREE-FOCK APPROXIMATION

The undoped cuprates show the antiferromagnetic (AF) long-range order at $T = 0$. It is known that the HFA works rather well in the AF phase even for the case of large Coulomb interaction between 3d electrons. Since the following analysis of RIXS is based on the HFA, we summarize the electronic structure within the HFA in this section. The unit cell in the AF phase contains six orbitals for each spin, as shown in Fig. 1. Introducing the Fourier transform in the magnetic Brillouin zone (BZ), we define the single-particle Green's function for six orbitals in a matrix form,

$$[\hat{G}^\sigma(\mathbf{k}, \omega)]_{\mu\nu} = -i \int \langle T(A_{\mathbf{k}\mu\sigma}(t) A_{\mathbf{k}\nu\sigma}^\dagger(0)) \rangle e^{i\omega t} dt. \quad (3.1)$$

where $A_{\mathbf{k}\mu\sigma}$ represents the annihilation operator of electron with the orbital at site μ in the unit cell. For example, at Cu sites ($\mu = 1$, and 4), it is given by

$$A_{\mathbf{k}\mu\sigma} \equiv d_{\mathbf{k}\sigma} = \sqrt{\frac{2}{N}} \sum_i d_{i\sigma} e^{i\mathbf{k}\mathbf{r}_i}, \quad (3.2)$$

with i running over the sites “ μ ” of $N/2$ unit cells.

Applying the equation of motion method to the Green’s functions, we obtain the relation,

$$(\omega \hat{I} - \hat{J}^\sigma(\mathbf{k})) \hat{G}^\sigma(\mathbf{k}, \omega) = \hat{I}, \quad (3.3)$$

where \hat{I} is the unit matrix, and $\hat{J}^\sigma(\mathbf{k})$ is given by

$$\begin{pmatrix} \epsilon_d + U_d n_{-\sigma}^A & t_d e^{i\frac{k_x}{2}} & -t_d e^{i\frac{k_y}{2}} & 0 & -t_d e^{-i\frac{k_x}{2}} & t_d e^{-i\frac{k_y}{2}} \\ & \epsilon_p & -2t_p \cos(\frac{k_x}{2} - \frac{k_y}{2}) & -t_d e^{i\frac{k_y}{2}} & 0 & 2t_p \cos(\frac{k_x}{2} + \frac{k_y}{2}) \\ & & \epsilon_p & t_d e^{i\frac{k_y}{2}} & 2t_p \cos(\frac{k_x}{2} + \frac{k_y}{2}) & 0 \\ & & & \epsilon_d + U_d n_{-\sigma}^B & t_d e^{i\frac{k_x}{2}} & -t_d e^{i\frac{k_y}{2}} \\ & & & & \epsilon_p & -2t_p \cos(\frac{k_x}{2} - \frac{k_y}{2}) \\ & & & & & \epsilon_p \end{pmatrix}, \quad (3.4)$$

with

$$n_\sigma^A = \frac{2}{N} \sum_{\mathbf{k}} \int [\hat{G}^\sigma(\mathbf{k}, \omega)]_{11} e^{i\omega 0^+} \frac{d\omega}{2\pi}, \quad n_\sigma^B = \frac{2}{N} \sum_{\mathbf{k}} \int [\hat{G}^\sigma(\mathbf{k}, \omega)]_{44} e^{i\omega 0^+} \frac{d\omega}{2\pi}. \quad (3.5)$$

Since $n_\sigma^B = n_{-\sigma}^A$, we may put

$$n_{\uparrow\downarrow}^A = \frac{1}{2}(n \pm m), \quad n_{\uparrow\downarrow}^B = \frac{1}{2}(n \mp m). \quad (3.6)$$

Lower triangle components are the Hermitian conjugates to the upper triangle components, which are omitted in Eq. (3.4). The $\hat{J}^\sigma(\mathbf{k})$ is diagonalized by an unitary matrix $\hat{U}^\sigma(\mathbf{k})$, that is, $[\hat{U}^{-1} \hat{J} \hat{U}]_{jj'} = E_j(\mathbf{k}) \delta_{jj'}$. Then the Green’s function is expressed as

$$\hat{G}^\sigma(\mathbf{k}, \omega) = U^\sigma(\mathbf{k}) \hat{D}(\mathbf{k}, \omega) U^\sigma(\mathbf{k})^{-1}, \quad (3.7)$$

with

$$[\hat{D}(\mathbf{k}, \omega)]_{jj'} = \frac{1}{\omega - E_j(\mathbf{k}) \pm i\delta} \delta_{jj'}. \quad (3.8)$$

Figure 3 shows the dispersion relation $E_j(\mathbf{k})$ as a function of \mathbf{k} along symmetry lines. The conduction band and the top of the valence band may be called the “upper Hubbard” band and the “charge transfer” band, respectively.

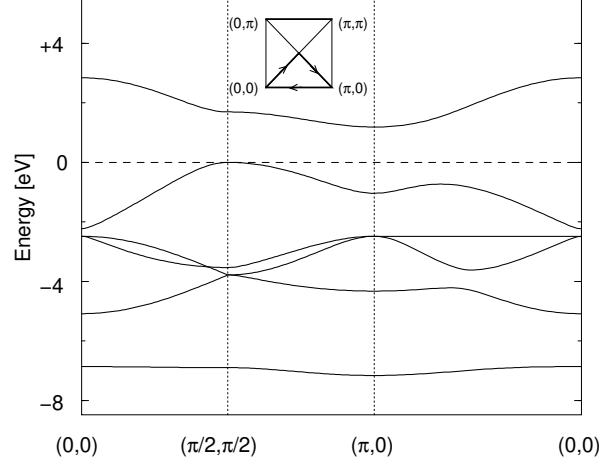


FIG. 3: Dispersion relation of Cu3d-O2p bands along symmetry lines in the Brillouin zone.

IV. BORN APPROXIMATION FOR RIXS SPECTRA

We consider the process that an electron-hole pair is singly created to screen the core-hole potential. The multiple-scattering effect beyond the Born approximation is neglected. Figure 4 displays the corresponding diagrams, where the shaded part represents the Keldysh-type Green's function,

$$Y_{\mu'\sigma',\mu\sigma}^{+-}(\mathbf{q}, s' - s) = \int Y_{\mu'\sigma',\mu\sigma}^{+-}(\mathbf{q}, \omega) e^{-i\omega(s'-s)} \frac{d\omega}{2\pi} \quad (4.1)$$

$$= \langle \rho_{\mathbf{q}\mu'\sigma'}(s') \rho_{-\mathbf{q}\mu\sigma}(s) \rangle, \quad (4.2)$$

with

$$\rho_{\mathbf{q}\mu\sigma} = \sqrt{\frac{2}{N}} \sum_{\mathbf{k}} d_{\mathbf{k}+\mathbf{q}\mu\sigma}^{\dagger} d_{\mathbf{k}\mu\sigma}. \quad (4.3)$$

The momentum conservation requires the relation $\mathbf{q} = \mathbf{q}_i - \mathbf{q}_f$, and \mathbf{k} runs over the magnetic first BZ. The superscripts + and - stand for the backward and outward time legs, respectively.¹⁸ In the lowest order, it is given by

$$Y_{\mu'\sigma',\mu\sigma}^{+- (0)}(\mathbf{q}, s' - s) = \frac{2}{N} \sum_{\mathbf{k}} \langle d_{\mathbf{k}+\mathbf{q}\mu'\sigma'}(s') d_{\mathbf{k}+\mathbf{q}\mu\sigma}^{\dagger}(s) \rangle \langle d_{\mathbf{k}\mu'\sigma'}^{\dagger}(s') d_{\mathbf{k}\mu\sigma}(s) \rangle, \quad (4.4)$$

and thereby

$$\begin{aligned} Y_{\mu'\sigma',\mu\sigma}^{+- (0)}(\mathbf{q}, \omega) &= \delta_{\sigma\sigma'} \sum_{\mathbf{k}} \sum_{j,j'} \delta(\omega - E_j([\mathbf{k} + \mathbf{q}]) + E_j(\mathbf{k})) [1 - n_{j'}([\mathbf{k} + \mathbf{q}])] n_j(\mathbf{k}) \\ &\times \tilde{U}_{\mu'j'}^{\sigma}([\mathbf{k} + \mathbf{q}]) \tilde{U}_{\mu j}^{\sigma*}([\mathbf{k} + \mathbf{q}]) U_{\mu j}^{\sigma}(\mathbf{k}) U_{\mu'j}^{\sigma*}(\mathbf{k}), \end{aligned} \quad (4.5)$$

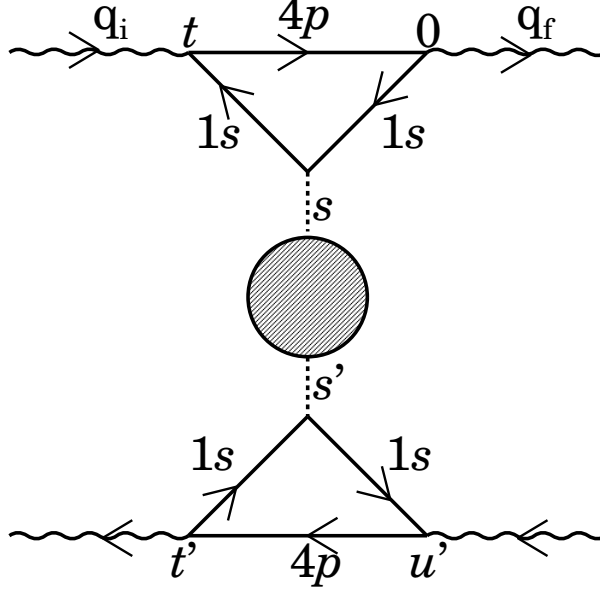


FIG. 4: Diagrams for the RIXS intensity within the Born approximation. The dotted lines represent the core-hole potential. The shaded part represents the Keldysh-type Green's function, which connects the outward time leg on the top half and the backward time leg on the bottom half.

where j and j' stand for energy eigenstates, and $[\mathbf{k} + \mathbf{q}]$ is the reduced value of $\mathbf{k} + \mathbf{q}$ into the magnetic first BZ by a reciprocal lattice vector \mathbf{G} , that is, $\mathbf{k} + \mathbf{q} = [\mathbf{k} + \mathbf{q}] + \mathbf{G}$. Since two Cu sites in the unit cell are involved to excite an electron-hole pair, phase factor $e^{i\mathbf{G}\mathbf{a}}$ is attached to the wave function at the B site,

$$\tilde{U}_{\mu j}^{\sigma}([\mathbf{k} + \mathbf{q}]) = e^{i\mathbf{G}\mathbf{a}} U_{\mu j}^{\sigma}([\mathbf{k} + \mathbf{q}]) \quad \text{for } \mu = 4, \quad (4.6)$$

where $\mu = 4$ corresponds to the Cu B site, and $\mathbf{a} (\equiv (a, 0))$ represents a position of the B site relative to the A site in the unit cell.

The product of Green's functions of the $4p$ electron and the core hole gives simply a factor $\exp[i(\epsilon_{4p}^{\eta}(\mathbf{p}) - \epsilon_{1s} - i\Gamma_{1s} - \omega_i)t]$ on the outward time leg and a factor $\exp[-i(\epsilon_{4p}^{\eta}(\mathbf{p}) - \epsilon_{1s} + i\Gamma_{1s} - \omega_i)(t' - u')]$ on the backward time leg, where Γ_{1s} is a lifetime broadening width of the $1s$ core hole. In a conventional calculation based on the Fourier transforms, this feature is hidden. This property will be fully utilized in the study of the multiple scattering effect in the next section. The Keldysh Green's function carries the time dependent factor $e^{i\omega s}$ to the outward time leg and $e^{-i\omega s'}$ to the backward time leg. Note that the core-hole potential

works only in intervals $[t, 0]$ and $[t', u']$. Integrating the time factor combined to the above product of Green's functions, with respect to s and t in the region of $t < s < 0$, $-\infty < t < 0$, we obtain

$$\begin{aligned} L_B^\eta(\omega_i; \omega) &\equiv V \int_{-\infty}^0 dt \sum_{\mathbf{p}} \exp[i(\epsilon_{4p}^\eta(\mathbf{p}) - \epsilon_{1s} - i\Gamma_{1s} - \omega_i)t] \int_t^0 ds e^{i\omega s} \\ &= \int \frac{V \rho_{4p}^\eta(\epsilon) d\epsilon}{(\omega_i + \epsilon_{1s} + i\Gamma_{1s} - \epsilon)(\omega_i - \omega + \epsilon_{1s} + i\Gamma_{1s} - \epsilon)}. \end{aligned} \quad (4.7)$$

Here the sum over $4p$ states is replaced by the integration of the $4p$ DOS projected onto the η ($= x, y, z$) symmetry, $\rho_{4p}^\eta(\epsilon)$. A similar factor has been derived in third-order perturbation theory by Abbamonte et al.¹⁹ The integration with respect to s' and t' in the backward time leg gives the term complex-conjugate to Eq. (4.7). The integration with respect to u' give the energy conservation factor, which guarantees that ω in Eq. (4.7) is the energy loss, $\omega = \omega_i - \omega_f$.

We evaluate the higher-order effect on $Y_{\mu'\sigma',\mu\sigma}^{+-}(q)$ ($q \equiv (\mathbf{q}, \omega)$) within the RPA. Figure 5 shows the corresponding diagram. Collecting up the ladder diagrams, we obtain

$$Y_{\mu'\sigma',\mu\sigma}^{+-}(q) = \sum_{\mu_1\sigma_1\mu_2\sigma_2} \Lambda_{\mu_1\sigma_1,\mu'\sigma'}^*(q) Y_{\mu_1\sigma_1,\mu_2\sigma_2}^{+- (0)}(q) \Lambda_{\mu_2\sigma_2,\mu\sigma}(q), \quad (4.8)$$

where

$$\Lambda_{\mu_1\sigma_1,\mu_2\sigma_2}(q) = \left[I - \hat{U}_d \hat{F}(q) \right]_{\mu_1\sigma_1,\mu_2\sigma_2}^{-1}, \quad (4.9)$$

with

$$\hat{F}(q) = \begin{pmatrix} F_{11}^\uparrow(q) & 0 & F_{14}^\uparrow(q) & 0 \\ 0 & F_{11}^\downarrow(q) & 0 & F_{14}^\downarrow(q) \\ F_{41}^\uparrow(q) & 0 & F_{44}^\uparrow(q) & 0 \\ 0 & F_{41}^\downarrow(q) & 0 & F_{44}^\downarrow(q) \end{pmatrix}, \quad (4.10)$$

$$\hat{U}_d = \begin{pmatrix} 0 & U_d & 0 & 0 \\ U_d & 0 & 0 & 0 \\ 0 & 0 & 0 & U_d \\ 0 & 0 & U_d & 0 \end{pmatrix}. \quad (4.11)$$

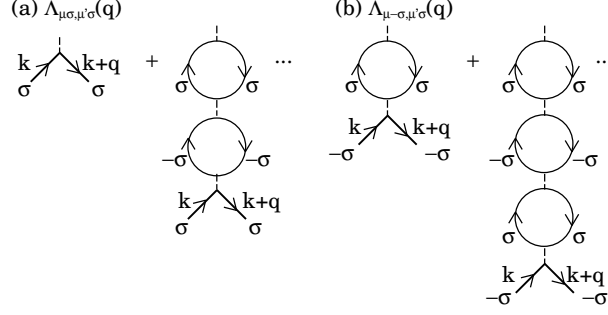


FIG. 5: Vertex function within the RPA; (a) the channel keeping spin, and (b) the channel reversing spin. Broken lines between bubbles represent the 3d Coulomb interaction, which is effective only between 3d electrons with opposite spins.

Here the polarization propagator $F_{\mu\mu'}^\sigma(q)$ is given by

$$\begin{aligned}
F_{\mu\mu'}^\sigma(q) &= -i \frac{2}{N} \sum_{\mathbf{k}} \int \frac{dk_0}{2\pi} G_{\mu\mu'}^\sigma(\mathbf{k}, k_0) G_{\mu'\mu}^\sigma(\mathbf{k} + \mathbf{q}, k_0 + \omega) \\
&= \frac{2}{N} \sum_{\mathbf{k}} U_{\mu j}^\sigma(\mathbf{k}) U_{\mu' j'}^{\sigma*}(\mathbf{k}) \tilde{U}_{\mu' j'}^\sigma([\mathbf{k} + \mathbf{q}]) \tilde{U}_{\mu j}^{\sigma*}([\mathbf{k} + \mathbf{q}]) \\
&\quad \times \left[\frac{n_j(\mathbf{k})[1 - n_{j'}([\mathbf{k} + \mathbf{q}])]}{\omega - E_{j'}([\mathbf{k} + \mathbf{q}]) + E_j(\mathbf{k}) + i\delta} - \frac{n_{j'}([\mathbf{k} + \mathbf{q}])[1 - n_j(\mathbf{k})]}{\omega - E_{j'}([\mathbf{k} + \mathbf{q}]) + E_j(\mathbf{k}) - i\delta} \right]. \quad (4.12)
\end{aligned}$$

Combining all these relations together, we finally obtain an expression of the RIXS intensity,

$$\begin{aligned}
W(q_i, \alpha_i; q_f, \alpha_f) &= 2\pi \frac{|w|^4}{4\omega_i\omega_f} \sum_{\mathbf{k} j j'} \sum_{\mu\sigma\mu'\sigma'} \sum_{\mu_1\mu_2\bar{\sigma}} \delta(\omega + E_j(\mathbf{k}) - E_{j'}([\mathbf{k} + \mathbf{q}])) n_j(\mathbf{k})[1 - n_{j'}([\mathbf{k} + \mathbf{q}])] \\
&\quad \times \Lambda_{\mu_1\bar{\sigma}, \mu'\sigma'}^*(q) U_{\mu_2 j}^{\sigma'}(\mathbf{k}) U_{\mu_1 j}^{\bar{\sigma}*}(\mathbf{k}) \tilde{U}_{\mu_1 j}^{\bar{\sigma}}([\mathbf{k} + \mathbf{q}]) \tilde{U}_{\mu_2 j}^{\sigma*}([\mathbf{k} + \mathbf{q}]) \Lambda_{\mu_2\bar{\sigma}, \mu\sigma}(q) \\
&\quad \times \left| \sum_{\eta} e_{\eta}^{(\alpha)} L_B^{\eta}(\omega_i; \omega) e_{\eta}^{(\alpha')} \right|^2, \quad (4.13)
\end{aligned}$$

where the incident photon has the momentum and energy $q_i = (\mathbf{q}_i, \omega_i)$, polarization $\mathbf{e}^{(\alpha_i)}$, and the scattered photon has the momentum and energy $q_f = (\mathbf{q}_f, \omega_f)$, polarization $\mathbf{e}^{(\alpha_f)}$. The transfer of momentum and energy is denoted as $\mathbf{q} = \mathbf{q}_i - \mathbf{q}_f$, $\omega = \omega_i - \omega_f$.

We have already reported the same formula without detailed derivation in Ref. 14. In that study, we calculated the RIXS spectra of La_2CuO_4 by assuming the two-dimensional cosine dispersion for the 4p band and tuning the incident photon energy to excite the core electron to the peak of the 4p density of states (DOS). We improve the treatment by using the realistic 4p-DOS calculated with the LDA. Although the LDA fails to predict the AF insulating

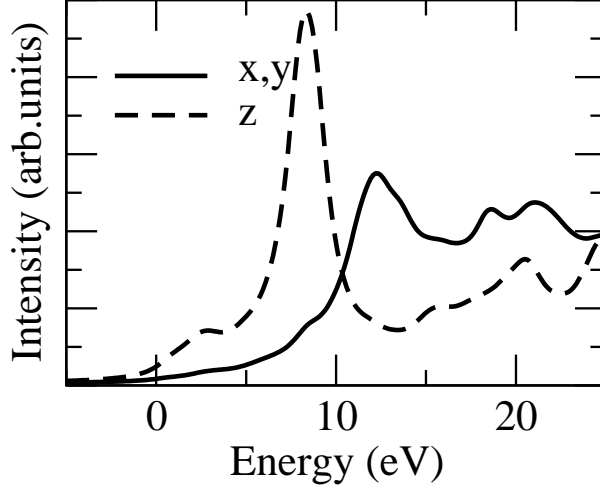


FIG. 6: Density of states for the $4p$ band convoluted with the Lorentzian function with HMF $\Gamma = 2\Gamma_{1s} = 1.6$ eV. The origin of energy corresponds to the bottom of the $4p$ band.

ground state, the $4p$ band is expected to be properly described because of weak correlation in wide bands. Figure 6 displays the $4p$ -DOS convoluted by the Lorentzian function with the half maximum full width (HMF Γ) $2\Gamma_{1s} = 1.6$ eV. Reflecting the tetragonal structure, the p_z -symmetric DOS is found quite different from the p_x - and p_y -symmetric DOS's. Since the experiment by Kim *et al.* has been performed with the polarization along the z axis, we concentrate our calculation to the p_z -symmetric DOS.

We calculate the RIXS intensity from Eq. (4.13) by tuning the incident photon energy at the peak of the p_z -DOS, the δ -function is replaced by the Lorentzian function with HMF $\Gamma = 0.2$ eV in order to take account of the instrumental resolution. Figure 7 shows the calculated spectra as a function of energy loss for momentum transfer $(0,0)$, $(\pi,0)$, and (π,π) . The present result using the realistic $4p$ -DOS is nearly the same as our previous one¹⁴ using a two-dimensional cosine dispersion for the $4p$ band. We obtain the spectra consisting of two peaks at about 2 eV and 5 eV as a function of energy loss, which shapes move with changing momenta in good agreement with the experiment. The 2eV-peak is assigned to the excitation from the charge transfer band to the upper Hubbard band. The 2eV-peak at $(0,0)$ is considerably enhanced while that at (π,π) is considerably suppressed by the vertex function of RPA in agreement with the experiment. As already emphasized in our previous paper,¹⁴ the inter-site correlation reinforced by the RPA is quite important for the quantitative understanding of the RIXS spectra. The difference between the present

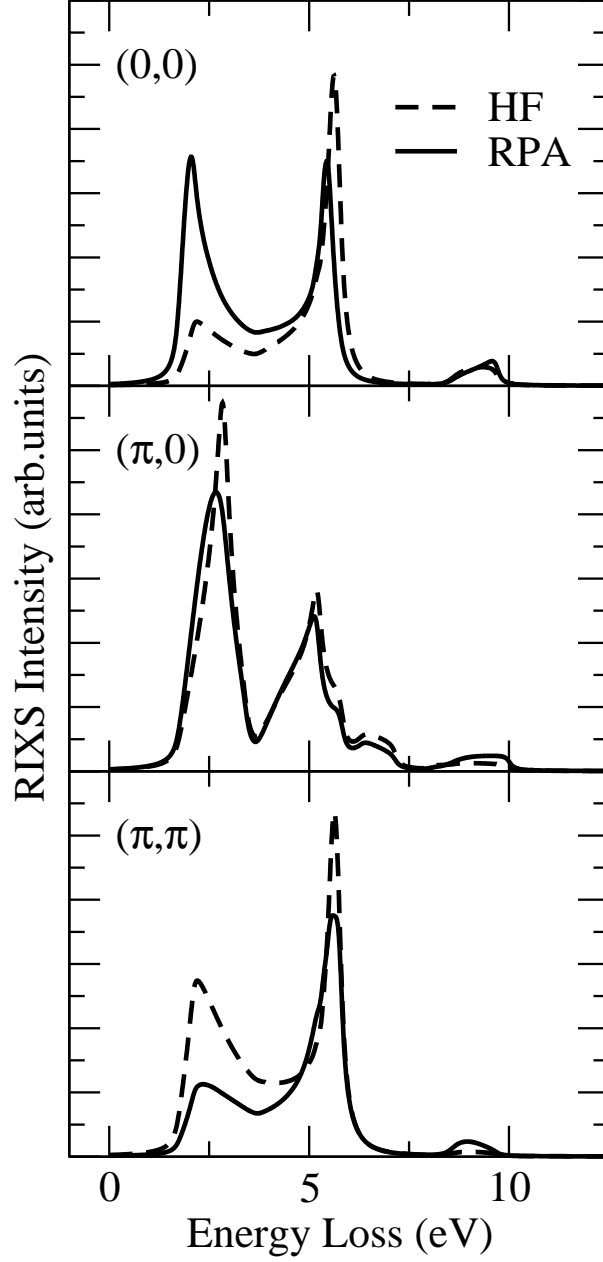


FIG. 7: RIXS spectra as a function of energy loss $\omega = \omega_i - \omega_f$, within the Born approximation. Momentum transfer is $(0,0)$, $(\pi,0)$, and (π,π) . The incident photon has the z -polarization and the energy corresponding to the excitation from the $1s$ core to the peak of the p_z -DOS. The dotted and solid lines are the results of the HFA and RPA, respectively.

and the previous results is that the 2eV-peak is a little enhanced relative to the 5eV-peak in the present result.

V. MULTIPLE SCATTERING BY THE CORE-HOLE POTENTIAL

Since the $1s$ -core hole potential is rather strong, many electron-hole pairs may be created in the $\text{Cu}3d\text{-O}2p$ bands in order to screen the potential. This process may influence not only the absorption spectra but also the RIXS spectra. It is known in metallic systems that the creation of infinite number of electron-hole pairs leads to “singular” behavior in the absorption spectra.^{16,20} In insulating systems, however, the number of electron-hole pairs is limited due to the finite energy gap, and the singularity would not come out. Under this condition, we calculate the RIXS and absorption spectra on the basis of the time representation developed by Noziere and de Dominicis.¹⁶

Since the potential is localized at Cu sites, it is convenient to introduce the one-electron Green’s function for the $3d$ electron localized at the μ -th site ($\mu = 1$, and 4),

$$\varphi_{\mu\sigma}(s_2, s_1) = -i\langle T(d_{\mu\sigma}(s_2)d_{\mu\sigma}^\dagger(s_1)) \rangle. \quad (5.1)$$

Here the core-hole potential works only between the time interval $[t, 0]$, and $t < s_1, s_2 < 0$. Figure 8 shows a diagram contributing to $\varphi_{\mu\sigma}(s_2, s_1)$. Collecting similar diagrams, we obtain the Dyson equation

$$\varphi_{\mu\sigma}(s_2, s_1) = G_{\mu\sigma}^{(0)}(s_2 - s_1) - V \int_t^0 G_{\mu\sigma}^{(0)}(s_2 - s_3) \varphi_{\mu\sigma}(s_3, s_1) ds_3, \quad (5.2)$$

where $G_{\mu\sigma}^{(0)}(s)$ represents the unperturbed local Green’s function, which is given by

$$G_{\mu\sigma}^{(0)}(s) = (-i) \frac{2}{N} \sum_{\mathbf{k}j} |U_{\mu j}^\sigma(\mathbf{k})|^2 (1 - n_j(\mathbf{k})) e^{-iE_j(\mathbf{k})s}, \quad s > 0, \quad (5.3)$$

$$= i \frac{2}{N} \sum_{\mathbf{k}j} |U_{\mu j}^\sigma(\mathbf{k})|^2 n_j(\mathbf{k}) e^{-iE_j(\mathbf{k})s}, \quad s < 0. \quad (5.4)$$

In metallic systems, $G_{\mu\sigma}^{(0)}(s)$ contains a singular term behaving as $\sim 1/s$, and the Dyson equation becomes a singular integral equation, which needs special care.¹⁶ On the other hand, in an insulating system we are dealing with, such singular terms would not exist in $G_{\mu\sigma}^{(0)}(s)$ due to the energy gap. In addition, the solutions for large values of $|t|$ are less important in the absorption coefficient and the RIXS spectra, since the finite core-hole life time reduces their contributions. Therefore, we can numerically solve the integral equation Eq. (5.2) in the finite interval $[t, 0]$ by dividing the interval into small widths. We set the maximum value of $|t|$ by 12 (eV)^{-1} and each width by 0.02 (eV)^{-1} . Note that we need the one-electron Green’s functions only for $s_2 = t$ or $s_1 = t$ in the later use.

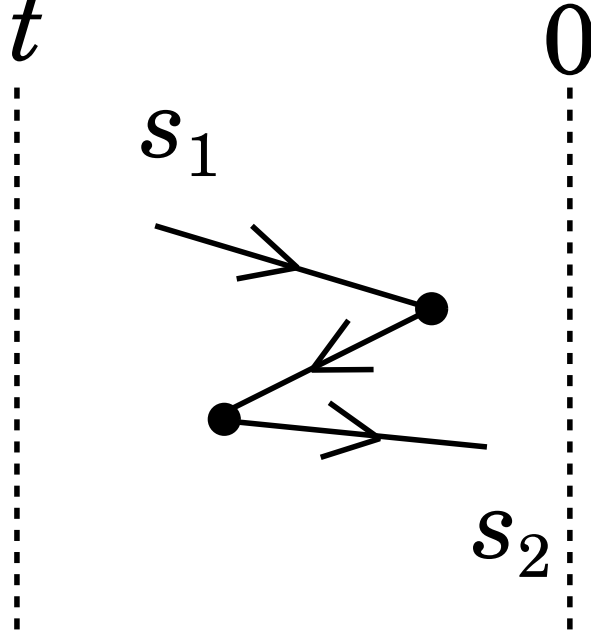


FIG. 8: Diagram for the one-electron Green's function $\varphi^\sigma(s_2, s_1)$. Solid circles represent the core hole potential working on.

A. Absorption coefficient

Before going to the RIXS spectra, we first formulate the absorption spectra. Let a photon have frequency ω_i and polarization direction η . Then, the absorption coefficient is calculated from

$$A_\eta(\omega_i) = \frac{1}{\pi} \text{Re} \int_{-\infty}^0 \langle H_x(0) H_x(t) \rangle dt. \quad (5.5)$$

Figure 9 shows a corresponding diagram, where the interaction between the core hole and the $4p$ electron is neglected. To screen the core-hole potential, electron-hole pairs are created. Without such bubble diagrams, the absorption coefficient is simply given by

$$\begin{aligned} A_\eta(\omega_i) &= \frac{1}{\pi} \frac{|w|^2}{2\omega_i} \text{Re} \sum_{\mathbf{k}} \int_{-\infty}^0 \exp\{i(\epsilon_{4p}^\eta(\mathbf{k}) - \epsilon_{1s} - i\Gamma_{1s} - \omega_i)t\} dt, \\ &= \frac{|w|^2 \Gamma_{1s}}{2\pi\omega_i} \int \frac{\rho_{4p}^\eta(\epsilon)}{(\omega_i - \epsilon + \epsilon_{1s})^2 + \Gamma_{1s}^2} d\epsilon. \end{aligned} \quad (5.6)$$

This is nothing but the $4p$ -DOS convoluted with the Lorentzian function with HMF Γ_{1s} .

The electron-hole pairs are treated on the basis of the linked cluster expansion. The

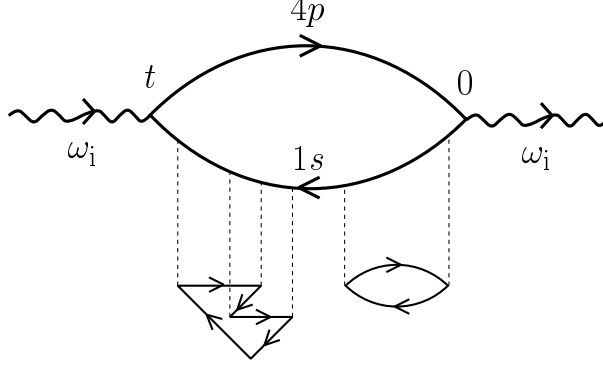


FIG. 9: Diagram for the absorption coefficient at the Cu K-edge. A photon enters with frequency ω and polarization η . The solid lines with “4p” and “1s” represent the Green’s function of the 4p electron and 1s-core hole, respectively. Other solid lines represent the local Green’s function. The dotted lines denote the core-hole potential.

contribution is simply given by a factor $e^{C(t)}$, where

$$C(t) = -\frac{1}{2}V^2 \sum_{\sigma} \int_t^0 \int_t^0 \varphi_{\mu\sigma}(s_2, s_1) G_{\mu\sigma}^{(0)}(s_1 - s_2) ds_1 ds_2. \quad (5.7)$$

In the actual calculation of $C(t)$, we numerically evaluate $dC(t)/dt$ from the relation

$$\frac{dC(t)}{dt} = \frac{1}{2}V^2 \sum_{\sigma} \int_t^0 [\varphi_{\mu\sigma}(t, s) G_{\mu\sigma}^{(0)}(s - t) + \varphi_{\mu\sigma}(s, t) G_{\mu\sigma}^{(0)}(t - s)] ds, \quad (5.8)$$

and then integrate this quantity with respect to t , instead of directly evaluating Eq. (5.7). The product of Green’s functions of the 4p electron and the core hole gives a factor $\exp[i(\epsilon_{4p}^{\eta}(\mathbf{k}) - \epsilon_{1s} - i\Gamma_{1s} - \omega_i)t]$, which is independent of times at which dotted lines are attached to the core hole line in Fig. 9. Therefore, the absorption coefficient is given by

$$A_{\eta}(\omega_i) = \frac{|w|^2}{2\pi\omega_i} \lim_{T \rightarrow -\infty} \text{Re}[K^{\eta}(\omega_i; T)], \quad (5.9)$$

with

$$\begin{aligned} K^{\eta}(\omega_i; T) &= \sum_{\mathbf{k}} \int_T^0 \exp[i(\epsilon_{4p}^{\eta}(\mathbf{k}) - \epsilon_{1s} - i\Gamma_{1s} - \omega_i)t] e^{C(t)} dt \\ &= \int \rho_{4p}^{\eta}(\epsilon) d\epsilon \int_T^0 \exp[i(\epsilon - \epsilon_{1s} - i\Gamma_{1s} - \omega_i)t] e^{C(t)} dt. \end{aligned} \quad (5.10)$$

We integrate numerically Eq. (5.10) up to $|T| = 12(eV)^{-1}$. Figure 10 shows the absorption coefficient thus evaluated for $V = 6$ eV, where the broken lines represent the quantity without

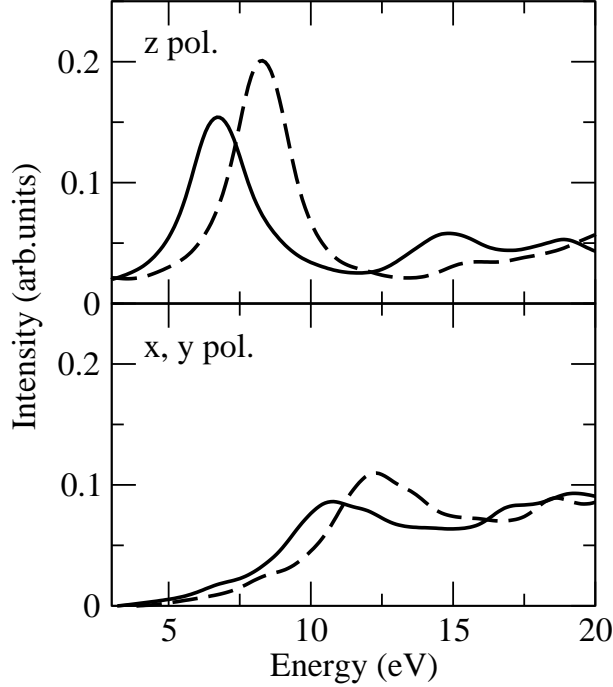


FIG. 10: Absorption coefficient for z , and x, y polarizations. The solid and broken lines represent the results with and without the screening by electron-hole pairs, respectively. $V = 6$ eV. The origin of energy corresponds to the excitation from the $1s$ core to the bottom of the $4p$ band.

taking account of the screening by electron-hole pairs (Eq. (5.6)). The K -edge peak moves about 2 eV to a lower energy position, which may be called as a “well-screened” peak. In addition, another peak appears at around 8 eV-higher position due to anti-screening, which may be called a “poorly-screened” peak. However, its peak is weak with a broad width and nearly merged into the background. Therefore, the screening effect may be, on the whole, taken into account by a renormalization of the core-level energy.

B. RIXS intensity

Confining ourselves within the HFA, we study the multiple scattering effect on the RIXS spectra in this subsection. Figure 11 shows the effect of the core-hole potential. Both the Born and the multiple scattering terms accompany the excitation of electron-hole pairs. The lines with E_1 and E_2 denote the factors $e^{-iE_1s_1}$ and $e^{iE_2s_2}$ coming from the Keldysh-type Green’s function, $Y_{\mu'\sigma',\mu\sigma}^{+- (0)}(q)$, which combines the outward and backward time legs. The product of Green’s functions of the $4p$ electron and the core hole, which is hidden in the

background, gives a factor $\exp[i(\epsilon_{4p}^\eta(\mathbf{k}) - \epsilon_{1s} - i\Gamma_{1s} - \omega_i)t]$. The electron-hole pairs give an extra factor $e^{C(t)}$, which is the same as in the absorption coefficient. Combining these factors, we obtain

$$L^\eta(\omega_i; E_1, E_2) = \sum_{\mathbf{k}} \int_{-\infty}^0 \exp[i(\epsilon_{4p}^\eta(\mathbf{k}) - \epsilon_{1s} - i\Gamma_{1s} - \omega_i)t] e^{C(t)} dt \\ \times \left\{ V \int_t^0 e^{i(E_2 - E_1)s} ds - V^2 \int_t^0 ds_2 \int_t^0 e^{iE_2 s_2} \varphi^\sigma(s_2, s_1) e^{-iE_1 s_1} ds_1 \right\} \quad (5.11)$$

$$= \int_{-\infty}^0 [K^\eta(\omega_i; -\infty) - K^\eta(\omega_i; t)] dt \\ \times \left\{ V e^{i(E_2 - E_1)t} - V^2 \int_t^0 [e^{iE_2 s} \varphi^\sigma(s, t) e^{-iE_1 t} + e^{iE_2 t} \varphi^\sigma(t, s) e^{-iE_1 s}] ds \right\}, \quad (5.12)$$

where $K^\eta(\omega_i; t)$ is defined by Eq. (5.10). The multiple scattering effect is included in $\varphi^\sigma(s_2, s_1)$. We finally obtain the formula of the RIXS intensity with replacing $L_B^\eta(\omega_i; \omega)$ by $L^\eta(\omega_i; E_j(\mathbf{k}), E_{j'}([\mathbf{k} + \mathbf{q}]))$ in Eq. (4.13).

On the basis of this formula, we calculate the RIXS spectra. We set the core-hole potential to be $V = 6$ eV, and tune the incident photon energy at the K -edge peak, which is shifted from the unscreened position. Figure 12 shows the calculated spectra in comparison with those by the Born approximation. The 2eV-peak is enhanced and the 5eV-peak is suppressed by the multiple scattering. This may be related to the fact that the incident photon energy is tuned to the “well screened” peak, where the excitation from the charge transfer band to the upper Hubbard band is most effective for screening. Nevertheless, the correction remains minor on the RIXS spectral shape. By comparison with the result in the previous section, the RPA correction is found more important.

VI. CONCLUDING REMARKS

We have developed a theory of the RIXS on the basis of the Keldysh Green’s function formalism. In this formula, we have described the electronic structure by the d - p model within the HFA, and have treated the electron correlation within the RPA. The RIXS spectra can be interpreted as a band-to-band transition reinforced by the RPA. We have analyzed the RIXS spectra of La_2CuO_4 using the realistic $4p$ -DOS, in good agreement with the experiment.

One of important approximations in our theory was the use of the Born approximation

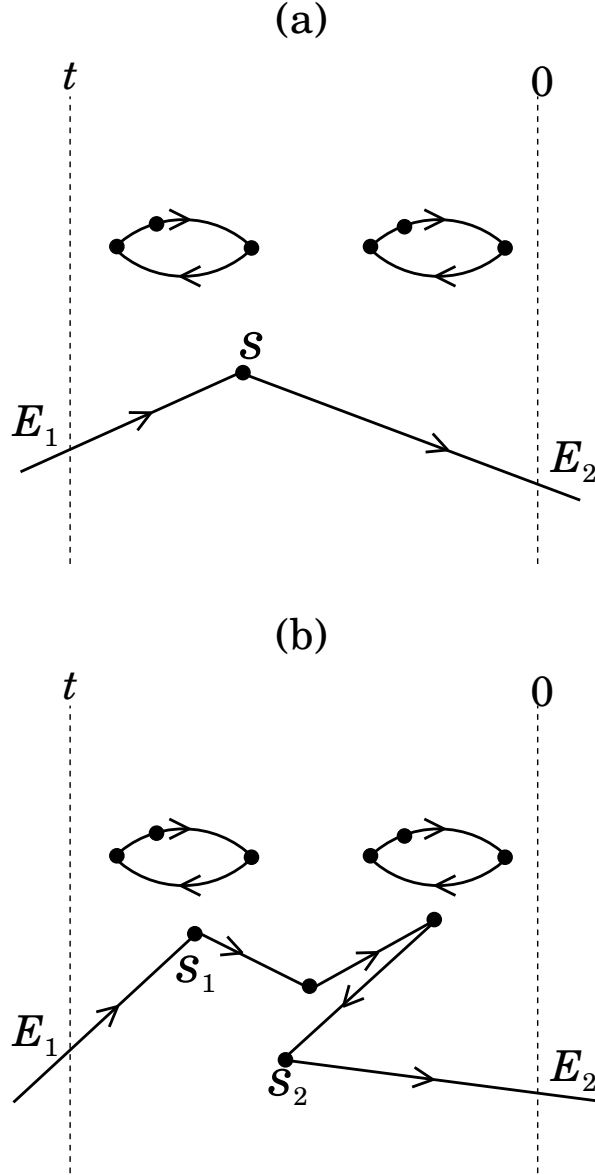


FIG. 11: Multiple scattering process for RIXS; (a) the Born term accompanying electron-hole pairs, and (b) a multiple scattering term. The solid lines represent the one-electron Green's function G_0^G and solid circles represent the core-hole potential causing scattering.

to treat the core-hole potential in the intermediate state. The multiple scattering effect may not be small, since the core-hole potential is by no means small. For evaluating the multiple-scattering effect, we have invented a numerical method along the line of Noziere and de Dominicis. In the absorption coefficient, we have found that the K -edge peak moves to a lower energy region due to screening (well-screened peak), and that another peak appears at a higher energy region due to anti-screening (poorly screened peak). However, the latter peak

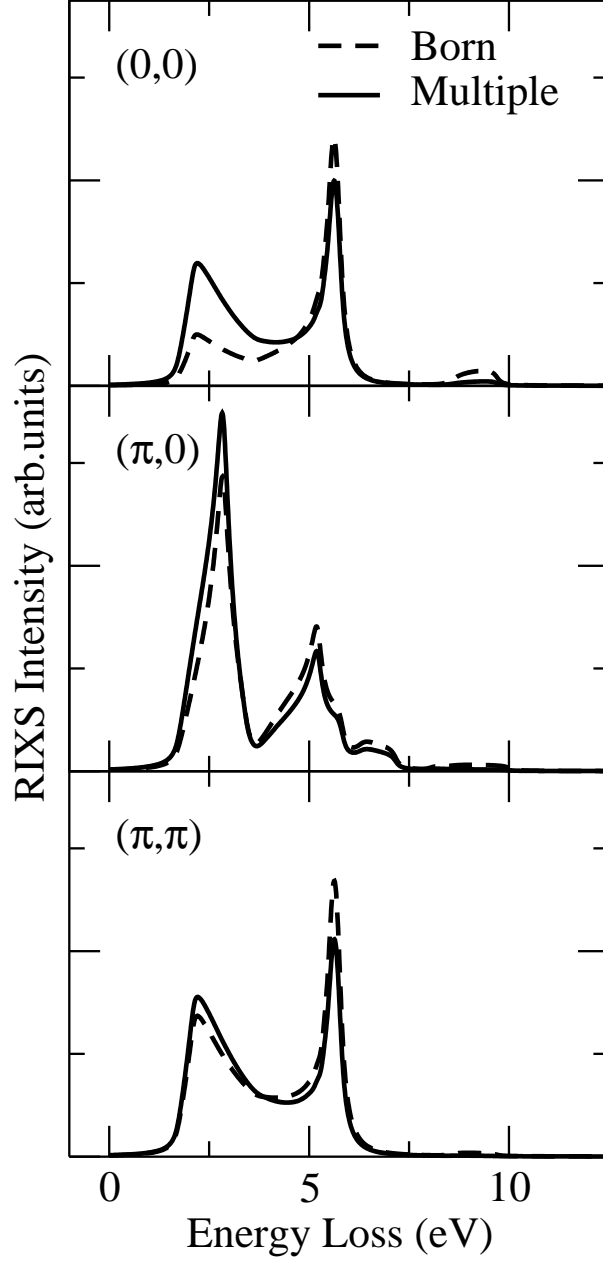


FIG. 12: RIXS spectra as a function of energy loss for momentum transfer $(0,0)$, $(\pi,0)$, and (π,π) , with including the multiple scattering effect (solid lines). The RPA correction is not included. The incident photon has the z -polarization and the energy tuned at the K -edge peak. The core-hole potential is set to be $V = 6$ eV. For comparison, the result within the Born approximation is displayed by the dotted lines (the incident energy is set to be the unscreened K -edge peak).

is weak with a broad width and nearly merged into the background. On the RIXS spectra, we have found that the multiple scattering modifies the spectral shape slightly. These findings suggest that the multiple scattering effect could be mainly included into a renormalization of the core-level energy, and partly justify the use of the Born approximation. The Born approximation is expected to work well in other insulating transition-metal compounds, such as NiO, LaMnO₃, etc. The present formula seems promising to analyze the RIXS spectra for such systems, because it can deal with multi-band tight-binding models in three dimensions.

The HFA and RPA are known to work well in the presence of the AF long-range order. Upon doping, the AF order is easily destroyed in cuprates. Recently the doping effects on the RIXS spectra have been observed in cuprates.^{21,22,23} In such a situation, the HFA no longer provides a good starting point, and we have to go beyond the HFA-RPA scheme. A study along this line is now under progress.

Acknowledgments

This work was partially supported by a Grant-in-Aid for Scientific Research from the Ministry of Education, Culture, Sports, Science, and Technology, Japan.

-
- ¹ C.-C. Kao, W. Caliebe, J. Hastings, and J.-M. Gillet, Phys. Rev. B **54**, 16361 (1996).
 - ² J. Hill, C.-C. Kao, W. A. L. Caliebe, M. Matsubara, A. Kotani, J. Peng, and R. Greene, Phys. Rev. Lett. **80**, 4976 (1998).
 - ³ M. Hasan, E. Isaacs, Z.-X. Shen, L. L. Miller, L. Tsutsui, T. Tohyama, and S. Maekawa, Science **288**, 1811 (2000).
 - ⁴ Y. J. Kim, J. P. Hill, C. A. Burns, S. Wakimoto, R. J. Birgeneau, D. Casa, T. Gog, and C. T. Venkataraman, Phys. Rev. Lett. **89**, 177003 (2002).
 - ⁵ T. Inami, T. Fukuda, J. Mizuki, S. Ishihara, H. Kondo, H. Nakao, T. Matsumura, K. Hirota, Y. Murakami, S. Maekawa, et al., Phys. Rev. B **67**, 045108 (2003).
 - ⁶ S. Suga, S. Imada, A. Higashiya, A. Shigemoto, S. Kasai, M. Sing, H. Fujiwara, A. Sekiyama, A. Yamasaki, C. Kim, et al., Phys. Rev. B **72**, 081101(R) (2005).

- ⁷ Y. J. Kim, J. P. Hill, H. Benthien, F. H. L. Essler, E. Jeckelmann, H. S. Choi, T. W. Noh, N. Motoyama, K. M. Kojima, S. Uchida, et al., Phys. Rev. Lett. **92**, 137402 (2004).
- ⁸ S. Uchida, T. Ido, H. Takagi, T. Arima, Y. Tokura, and S. Tajima, Phys. Rev. B **43**, 7942 (1991).
- ⁹ Y. Y. Wang, F. C. Zhang, V. P. Dravid, K. K. Ng, M. V. Klein, S. E. Schnatterly, and L. L. Miller, Phys. Rev. Lett. **77**, 1809 (1996).
- ¹⁰ K. Tsutsui, T. Tohyama, and S. Maekawa, Phys. Rev. Lett. **83**, 3705 (1999).
- ¹¹ K. Okada and A. Kotani, J. Phys. Soc. Jpn. **75**, 044702 (2006).
- ¹² K. Tsutsui, T. Tohyama, and S. Maekawa, Phys. Rev. Lett. **91**, 117001 (2003).
- ¹³ T. Nomura and J. Igarashi, J. Phys. Soc. Jpn. **73**, 1677 (2004).
- ¹⁴ T. Nomura and J. Igarashi, Phys. Rev. B **71**, 035110 (2005).
- ¹⁵ P. Noziere and E. Abrahams, Phys. Rev. B **10**, 3099 (1974).
- ¹⁶ P. Noziere and C. T. D. Dominicis, Phys. Rev. **178**, 1097 (1969).
- ¹⁷ M. S. Hybertsen and M. Schluter, Phys. Rev. B **39**, 9028 (1989).
- ¹⁸ L. D. Landau and E. M. Lifshitz, *Physical Kinetics* (Butterworth-Heinemann, Oxford, 1962), chap. 10.
- ¹⁹ P. Abbamonte, C. A. Burns, E. D. Isaacs, P. M. Platzman, L. L. Miller, S. W. Cheong, and M. V. Klein, Phys. Rev. Lett. **83**, 860 (1999).
- ²⁰ G. D. Mahan, Phys. Rev. **163**, 612 (1967).
- ²¹ K. Ishii, K. Tsutsui, Y. Endoh, T. Tohyama, K. Kuzushita, T. Inami, K. Ohwada, S. Maekawa, T. Masui, S. Tajima, et al., Phys. Rev. Lett. **94**, 187002 (2005).
- ²² K. Ishii, K. Tsutsui, Y. Endoh, T. Tohyama, S. Maekawa, M. Hoesch, K. Kuzushita, M. Tsubota, T. Inami, J. Mizuki, et al., Phys. Rev. Lett. **94**, 207003 (2005).
- ²³ Y. J. Kim, J. P. Hill, S. Komiya, Y. Ando, D. Casa, T. Gog, and C. T. Venkataraman, Phys. Rev. B **70**, 094524 (2004).